Research Square

Preprints are preliminary reports that have not undergone peer review.
They should not be considered conclusive, used to inform clinical practice,
or referenced by the media as validated information.

Increased Old Carbon Mobilization from Permafrost Ecosystems at a Decadal Scale

Allison K. Kelley

Allison.Kelley@nau.edu

Northern Arizona University https://orcid.org/0000-0001-6227-6529

Christopher Ebert

Northern Arizona University

Jonathon O'Donnell

National Park Service

Brett Poulin

University of California, Davis https://orcid.org/0000-0002-5555-7733

Emily Romano

Northern Arizona University

Ariella Thompson

Northern Arizona University

Alyson Welch

Northern Arizona University

Emma Lathrop

Northern Arizona University

Justin Ledman

Northern Arizona University

Edward Schuur

Northern Arizona Univeristy https://orcid.org/0000-0002-1096-2436

Physical Sciences - Article

Keywords:

Posted Date: June 8th, 2026

DOI: https://doi.org/10.21203/rs.3.rs-9581624/v1

License: This work is licensed under a Creative Commons Attribution 4.0 International License.
Read Full License

Additional Declarations: There is **NO** Competing Interest.

Increased Old Carbon Mobilization from Permafrost Ecosystems at a Decadal Scale

A.K. Kelley[1], C.H. Ebert[1], J.A. O'Donnell[2], B.A. Poulin[3], E. Romano[1], A. R. Thompson[1], A. Welch[1], E.R., Lathrop[1], J. Ledman[1], and E.A.G. Schuur[1]

[1]Northern Arizona University, Center for Ecosystem Science and Society & Department of Biological Sciences, Flagstaff AZ, 86011.

[2]National Park Service, Anchorage, AK, 99501

[3]Department of Environmental Toxicology, University of California, Davis, USA

Corresponding author: Allison K. Kelley (Allison.Kelley@nau.edu)

Permafrost soils store large reservoirs of organic carbon isolated from the modern carbon cycle for hundreds to thousands of years. Mobilization of old carbon to the atmosphere and aquatic systems has the potential to amplify climate warming through a permafrost-carbon feedback. Quantifying old carbon release through different ecosystem pathways over time is key to understanding the strength of this feedback. However, long-term observational records remain rare. Here we present a multi-decadal radiocarbon record of carbon dioxide (CO_2) from terrestrial systems and dissolved organic carbon (DOC) from aquatic systems across Alaskan permafrost landscapes. Radiocarbon measurements, which distinguish young, recently fixed carbon from older carbon, show a sustained and accelerating increase in the contribution of old carbon to all fluxes since the early 2000s. The shift toward older carbon was more pronounced in aquatic DOC than in terrestrial CO2 fluxes, likely reflecting greater mobilization of carbon from deeper, previously frozen soil horizons. The integration of old carbon across watersheds makes aquatic fluxes particularly sensitive indicators of landscape-scale permafrost carbon mobilization. This signal records decadal-scale change in ecosystem old carbon flux, pointing towards threshold change in these permafrost ecosystems. Together, this dataset provides direct evidence that warming is driving a persistent shift in carbon loss pathways and contributing to the permafrost-carbon feedback.

Permafrost regions in the northern hemisphere store a disproportionately large share of the world's soil organic carbon, accumulated over centuries to millennia[1–3]. However, rapid warming[4] has the potential to render this old carbon pool vulnerable to decomposition by microbes and release into the active carbon cycle[5]. The net release of permafrost carbon into the atmosphere has the potential to accelerate climate warming, which can be mitigated in part by increased plant growth and carbon uptake[3,6]. This permafrost carbon feedback[1,3] has been identified as one of the largest feedbacks to anthropogenic climate change, but also one where the magnitude is most uncertain[7,8]. Despite the potential importance of permafrost carbon for climate in a warmer world, observational evidence demonstrating the release of old carbon in ecosystem fluxes remains limited[3,9,10].

Tracking the release of old carbon as part of ecosystem carbon fluxes, such as DOC and CO_2, is possible using radiocarbon (^{14}C)[11–14]. Radiocarbon is a powerful tracer that records the time elapsed since carbon was incorporated by plant photosynthesis from the atmosphere into the ecosystem, providing a measure of carbon age and turnover in soils, plants, and ecosystem fluxes[15–18]. Relatively young surface soil and plant carbon reflect the contemporary atmospheric radiocarbon signal, which incorporates the legacy of mid-twentieth-century nuclear weapons testing and continued dilution from fossil fuel burning, as well as carbon exchange with the ocean and biosphere. In contrast, older carbon stored

for centuries to millennia and isolated from atmospheric exchange, such as permafrost carbon, is depleted in radiocarbon due to radioactive decay[19–23].

Radiocarbon measurements across ecosystem pools and fluxes illuminate carbon flow pathways and constrain turnover times[23]. Comparing radiocarbon values of carbon fluxes to the atmospheric baseline enables estimation of ecosystem carbon pool turnover including old carbon contribution[14,24–26]. Repeated observations through time further enable the detection of carbon cycle processes including ecosystem disequilibrium. This is when the rate of change through time in the radiocarbon of fluxes exceeds what steady-state turnover would predict and can provide direct evidence of increasing old carbon contribution to contemporary ecosystem fluxes[15].

Despite this potential to elucidate the permafrost carbon feedback, long-term observational constraints on permafrost carbon mobilization remain scarce because radiocarbon studies of ecosystem pools and fluxes have historically been limited by analytical cost, sample size requirements, and logistical challenges in remote Arctic environments, resulting in a reliance on short-term campaigns or isolated measurements[12,25,27,28]. Consequently, multi-decadal radiocarbon time series of carbon fluxes are rare yet invaluable for fingerprinting old carbon release from permafrost. Here, we present a 22-year radiocarbon timeseries of CO_2 and DOC measurements (n = 1,693) across a network of permafrost ecosystems in Interior Alaska. We combine terrestrial CO_2 and aquatic DOC flux records to determine the integrated landscape response, using both contemporary and historic samples. We applied isotope mixing models to separate contributions of old and young carbon pools to carbon flux pathways to determine decadal-scale changes. This unique long-term record enables direct assessment of shifts in old carbon mobilization and helps to identify environmental drivers. Together, these observations provide novel constraints on the dynamics of the permafrost carbon feedback and its role in accelerating Arctic and global climate change.

Carbon fluxes show accelerating radiocarbon depletion

The terrestrial CO_2 (soil respiration, ecosystem respiration) and aquatic DOC measurements, spanning increasing spatial integration from soil pore water to first-order (~0.5 m width) and second-order (~5–10 m width) streams, were concentrated at one intensive study site. Measurements culminated with regional-scale measurements of higher-order streams (>5-10m width) across the Yukon River basin. During the study period, the atmosphere radiocarbon signal declined at -3.8‰ yr^{-1} (2002 and 2024; Fig. 1), due to fossil fuel combustion[29,30] and all terrestrial and aquatic radiocarbon fluxes exhibited steeper negative trends than atmospheric radiocarbon. This is consistent with increasing contributions from older carbon pools to both aquatic and terrestrial fluxes over the study period, outpacing fossil fuel dilution in the atmosphere that imprints on young carbon.

Soil respiration (belowground CO_2 within the surface soil) and ecosystem respiration (total CO_2 leaving the ecosystem back to the atmosphere) declined at rates of -6.6 and 6.3‰ yr^{-1} (SE = 0.5 and 0.2, respectively; both $p<0.001$). These terrestrial fluxes differ in their relative contributions from plant metabolism vs soil organic matter decomposition, with soil respiration reflecting a greater proportion of the soil microbial signal relative to ecosystem respiration. Within DOC fluxes, the steepest declines were observed in soil pore water (-15.6‰ yr^{-1}, SE = 2.7, $p<0.001$), followed by higher-order streams (-12.2‰ yr^{-1}, SE = 1.3, $p<0.001$), second-order streams (-11.3‰ yr^{-1}, SE = 2.7, $p<0.01$) and first-order streams (-5.2‰ yr^{-1}, SE = 0.5, $p<0.001$).

Between terrestrial and aquatic flux types, radiocarbon decline was greatest in soil pore water and higher-order stream DOC, while CO_2 fluxes showed declines intermediate between atmosphere and most DOC values (Fig. S1). Pairwise comparisons revealed that DOC in soil pore water and higher-order streams declined significantly faster than first-order streams, and both CO_2 fluxes (BH-adjusted Z-test, $p<0.001$ for all three), despite wide 95% confidence intervals (Fig. S1). Second-order stream DOC declines were statistically similar to both the terrestrial CO_2 and DOC fluxes from other aquatic ecosystems.

Radiocarbon distributions of carbon fluxes, normalized to atmospheric radiocarbon in the year of sample collection ($\Delta\Delta^{14}C$), further revealed increasing contributions of older carbon over time (Fig. 1B). Early in the time series (2002-2013), fluxes exhibited $\Delta\Delta^{14}C$ distributions centered near zero, indicating dominance of fast-cycling, young carbon sources similar to the atmosphere. In later years (2014-2024), distributions shifted towards more negative $\Delta\Delta^{14}C$ values, reflecting progressive mobilization of older carbon. Figure 1B highlights these trends for fluxes with the longest records. The median apparent radiocarbon age became 320 years older (95% CI: 280 to 350 years) for ecosystem respiration and 650 years older (95% CI: 560 to 750 years) for soil respiration between periods (Fig. S2). DOC radiocarbon ages in higher order stream shifted 2,040 years older (95% CI: 980 to 2670 years). The oldest flux sample measured was a 2024 soil respiration sample with an apparent radiocarbon age of 6120 years before 1950.

Old carbon contributions increase over time

The radiocarbon values of DOC and CO_2 represent carbon mixtures of different ages. We defined two end members present in these mixtures: young carbon (median $\Delta^{14}C$ of 39±107‰, with a modern radiocarbon age, derived from surface soil 0-25cm) and old carbon (median $\Delta^{14}C$ of -442±182‰ and radiocarbon age of 5,000 years BP, derived from deeper soil 45-105cm; Fig. S3). Even in a steady-state system, fluxes include contributions from older carbon, with their smaller relative proportion reflecting the longer turnover times of these soil pools. By applying Bayesian isotope mixing models, we quantified how the proportions of young and old carbon changed over time, providing insight into temporal

variation in pool turnover. These mixing models ultimately revealed consistent increases in the relative contributions of old carbon across all measured flux types (Fig. 2, Table S2) and these trends were conserved even when the end-member values were perturbed in sensitivity tests (Fig. S4). At the start of the record, old carbon comprised less than 20% of all fluxes and by the end of the record, old carbon contributions had all increased by 37-80%. The posterior probability of an increase in old carbon contributions exceeded 99.9% for ecosystem respiration, soil respiration, and soil pore water DOC, with credible intervals entirely above zero. Stream fluxes showed consistent directional increases with posterior probabilities of 79 to 89%, though greater hydrologic variability and sparser sampling produced wider uncertainty in these fluxes.

At the intensive site scale, old carbon contributions increased most dramatically in the terrestrial, CO_2 flux pathways. By 2024, mean contributions (±SD) reached 62±10% in ecosystem respiration and 80±8% in soil respiration, up from less than 2% and 5% at the start of their respective records. These fluxes directly integrate soil profile respiration and thus reflect the increasing decomposition of deeper, older organic matter. Soil pore water, which represents lateral subsurface flow, similarly increased from 6% to 56±10% old carbon by 2024, consistent with deepening flow paths reaching older soil horizons as a result of permafrost degradation.

Downstream, first- and second-order streams draining the intensive, terrestrial measurement sites showed similar trajectories, reaching 50±24% and 48±33% old carbon respectively by the end of the time series, with wide uncertainty likely reflecting fewer observations of stream DOC radiocarbon and flow paths and dynamics of headwaters that influence C sources. Moving to a regional scale, higher-order streams across the Yukon River basin showed old carbon contributions nearly doubling from 20±8% (2002-2011) to 37±14% (2024), demonstrating that old carbon mobilization extends beyond a single site and reflects a consistent, system-wide shift across aquatic and terrestrial carbon export pathways over the past two decades.

Warming releases older carbon across terrestrial and aquatic fluxes

To evaluate drivers of change in old carbon contribution, we examined relationships between radiocarbon declines and air temperature. Radiocarbon values decreased with increased mean annual air temperature for all fluxes (Fig. 3), with slopes ranging from -0.15‰ °C^{-1} for ecosystem respiration to -0.57‰ °C^{-1} for first-order stream water. In each case, warmer years were associated with more negative $\Delta\Delta^{14}C$ values, indicating increased mobilization of older carbon pools under warmer conditions (all $p<0.0001$, except higher-order streams $p = 0.55$). The strongest temperature sensitivities were observed in the stream DOC fluxes, particularly first-order (slope = -0.57), suggesting that hydrologic pathways integrating deeper soil carbon pools may be especially responsive to warming.

Soil pore water showed an intermediate sensitivity (slope = -0.39), while the respiratory fluxes showed weaker but still significant relationships (soil respiration slope = -0.35, ecosystem respiration slope = -0.15).

Old aquatic fluxes reveal an enhanced signal of permafrost thaw

Soil pore water, perched directly atop the thawing permafrost table, likely represents the most source-proximal signal in this dataset, with minimal dilution by young, plant-derived inputs and direct connectivity to deepening active layer horizons. As the permafrost table thawed and receded further below ground over the course of this timeseries[31], pore water integrated progressively less surface soil and plant carbon and more carbon from the deepest accessible soil horizons. This signal is likely amplified during periods when the water table drops below the younger, organic surface layer, increasing contact with older mineral and permafrost-derived carbon[15,32]. Further, as this carbon moves laterally through the stream network as DOC, it may progressively mix with younger carbon from surface runoff, riparian soils, and autochthonous carbon, and be exposed to more in-stream processing[26,33,34]. Yet, radiocarbon declines in first- and second-order streams still significantly exceeded atmospheric decline, confirming that the old carbon signal observed in soil pore DOC is preserved during lateral transport, rather than being fully diluted by younger carbon inputs or lost to degradation.

Higher order streams as regional indicators of old carbon export

Ultimately, higher-order streams occupied a particularly valuable position in the carbon export continuum, showing pronounced $\Delta^{14}C$ declines (Fig. 1., Fig. S1) and the largest radiocarbon age shift of the aquatic fluxes by 2024 (Fig S2, Table S2). Regional streams integrate carbon mobilized across the full landscape with potentially less dilution by and more upstream degradation of young autotrophic sources[33,35,36], making them particularly sensitive indicators of permafrost carbon mobilization at the catchment scale. The old carbon signal accumulating in soil pore water and lower-order streams is largely absent from the predominantly young DOC export that characterizes large Arctic rivers[27,37,38], suggesting that this signal is progressively diluted or that old carbon is largely degraded as carbon moves through a river network. Higher-order streams appear to represent a critical window, where landscape-scale permafrost mobilization is still detectable, before that signal is lost within large rivers. This makes them particularly valuable observational targets, capturing a landscape-integrated permafrost signal that is neither as concentrated as source-proximal fluxes observed within soil pore water nor as diluted as major river export.

A persistent, multidecadal shift in old carbon release corresponding with warming air

temperatures

Radiocarbon depletion increased with annual air temperature across all fluxes (Fig. 3, S5, S6), consistent with deeper active layer thaw[39–41], enhanced microbial decomposition of previously frozen organic matter[42,43], and shifts in hydrologic connectivity that increase subsurface water contact with older carbon pools[44,45]. At this site, active layer depth increased from ~53 cm to ~98 cm between 2009 and 2024, with deepening accelerating from 2.6 cm yr^{-1} in the early record to 3.8 cm yr^{-1} after 2013, providing direct evidence that the thaw-driven exposure of older, deeper carbon pools accompanied the radiocarbon trends observed across fluxes[46]. Though regional active layer depth data are not available across the full watershed, the coherence of the old carbon signal in higher-order streams, which integrate inputs across a much larger drainage area, suggests that similar thaw dynamics are operating at the regional scale with warming (Fig. S6). This temperature dependence across such diverse flux types suggests that as the landscape warms, carbon that has been frozen and isolated from decomposition becomes increasingly accessible, and that signal propagates simultaneously through both terrestrial and aquatic fluxes.

The radiocarbon record presented here demonstrates an increasing old carbon signal across diverse terrestrial and aquatic ecosystem fluxes. Each flux began with lower modeled contributions of old carbon and ended the record with substantially higher contributions (Fig. 2). In CO_2 and DOC fluxes across stream networks, radiocarbon declined faster than the atmosphere (Fig. 1). The coherence across these fluxes, each integrating a different part of the ecosystem and hydrologic continuum, provides robust evidence that older carbon, deeper in the soil profile, is entering the contemporary carbon cycle and that this shift is persistent, not just episodic. While radiocarbon does not quantify total carbon mass transfer, it uniquely distinguishes whether ecosystem carbon fluxes reflect young carbon cycling within a steady-state system or old carbon representing a net addition to the contemporary carbon cycle. The persistent nature of this shift, corroborated across flux types spanning soil pore water to regional river basins, substantially strengthens the inference that old carbon mobilization is an ongoing and intensifying process across changing permafrost landscapes in Alaska.

Methods, Figures, Tables, and Extended Data for:

Increased Old Carbon Mobilization from Permafrost Ecosystems at a Decadal Scale

A.K. Kelley[1], C.H. Ebert[1], J.A. O'Donnell[2], B.A. Poulin[3], E. Romano[1], A. R. Thompson[1], A. Welch[1], E.R., Lathrop[1], J. Ledman[1], and E.A.G. Schuur[1]

[1]Northern Arizona University, Center for Ecosystem Science and Society & Department of Biological Sciences, Flagstaff AZ, 86011.

[2]National Park Service, Anchorage, AK, 99501

[3]Department of Environmental Toxicology, University of California, Davis, USA

Corresponding author: Allison K. Kelley (Allison.Kelley@nau.edu)

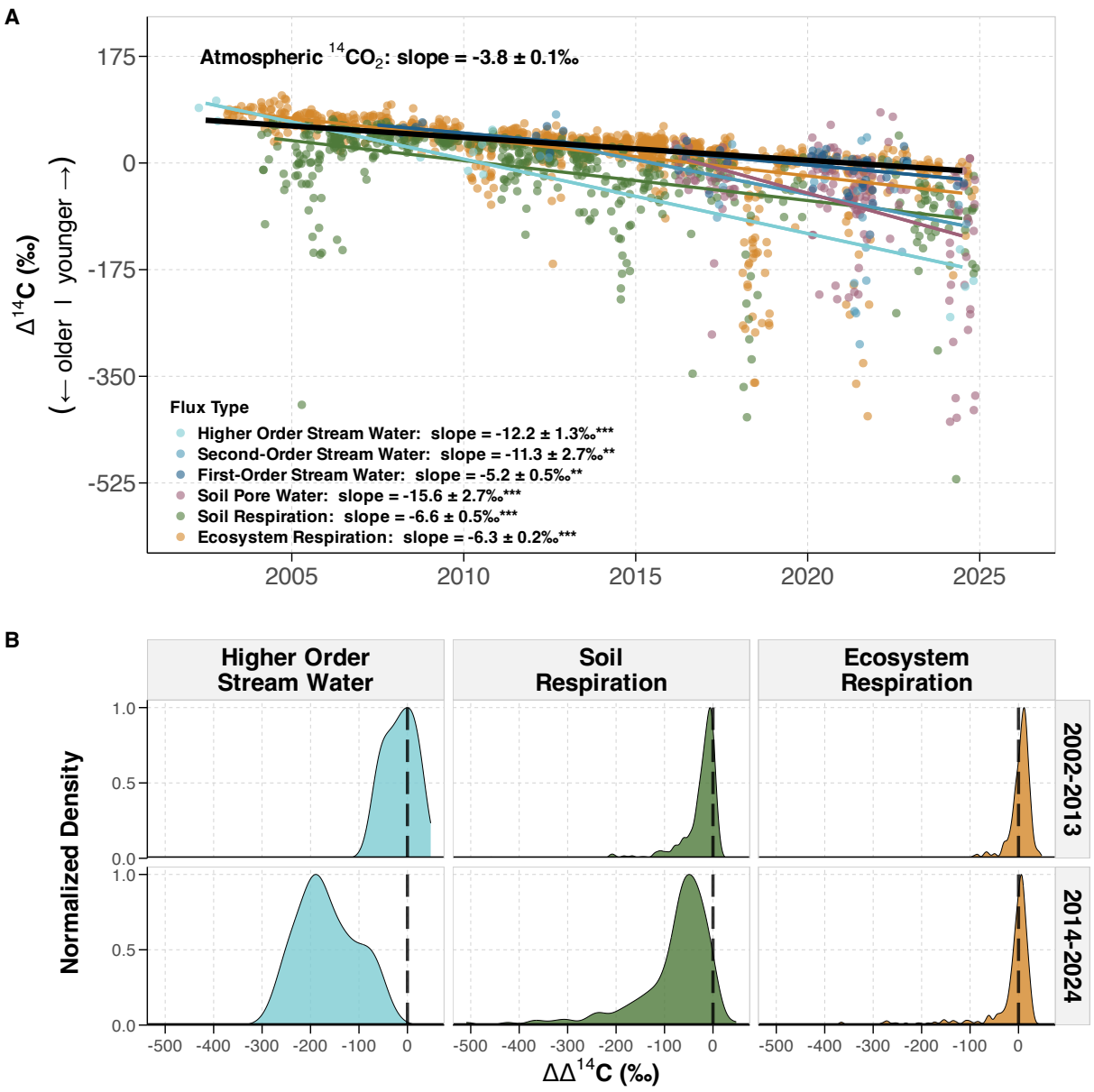


Figure 1: Radiocarbon signatures of carbon fluxes show an increasing influence of old carbon over time. *1A: Time series of $\Delta^{14}C$ values from carbon fluxes sampled between 2002 and 2024, alongside atmospheric $\Delta^{14}CO_2$. Colored lines indicate linear regressions with slope and p-value (***: <0.001, **: <0.01, *: <0.05) for each flux type: higher order streams (light blue), second-order streams (medium blue), first-order streams (dark blue), pore water (pink), ecosystem respiration (yellow), and soil respiration (green). 1B: Density plots of $\Delta\Delta^{14}C$ for three flux types with the longest timeseries, where $\Delta\Delta^{14}C$ represents the deviation from atmospheric radiocarbon in the year of sample collection to allow for the comparison across years. The vertical black dashed line indicates contemporary atmospheric $\Delta^{14}C$ normalized to zero.*

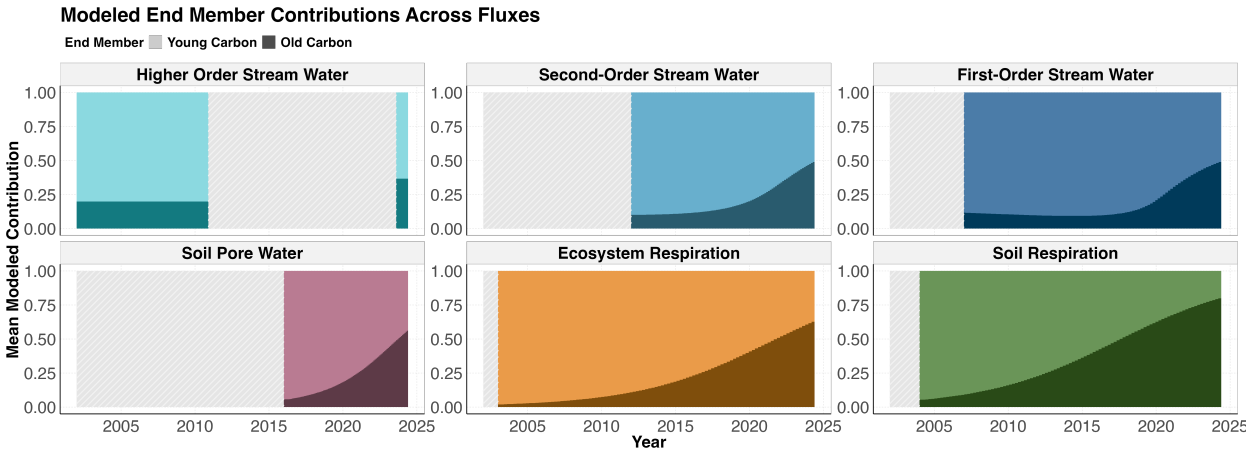


Figure 2: Modeled contributions of carbon sources to DOC and CO_2 fluxes.
Plots show relative contributions of young carbon and old carbon to the six flux types, estimated using a Bayesian isotope mixing model. Time series are shown from 2002-2024 with shaded grey indicating no data.

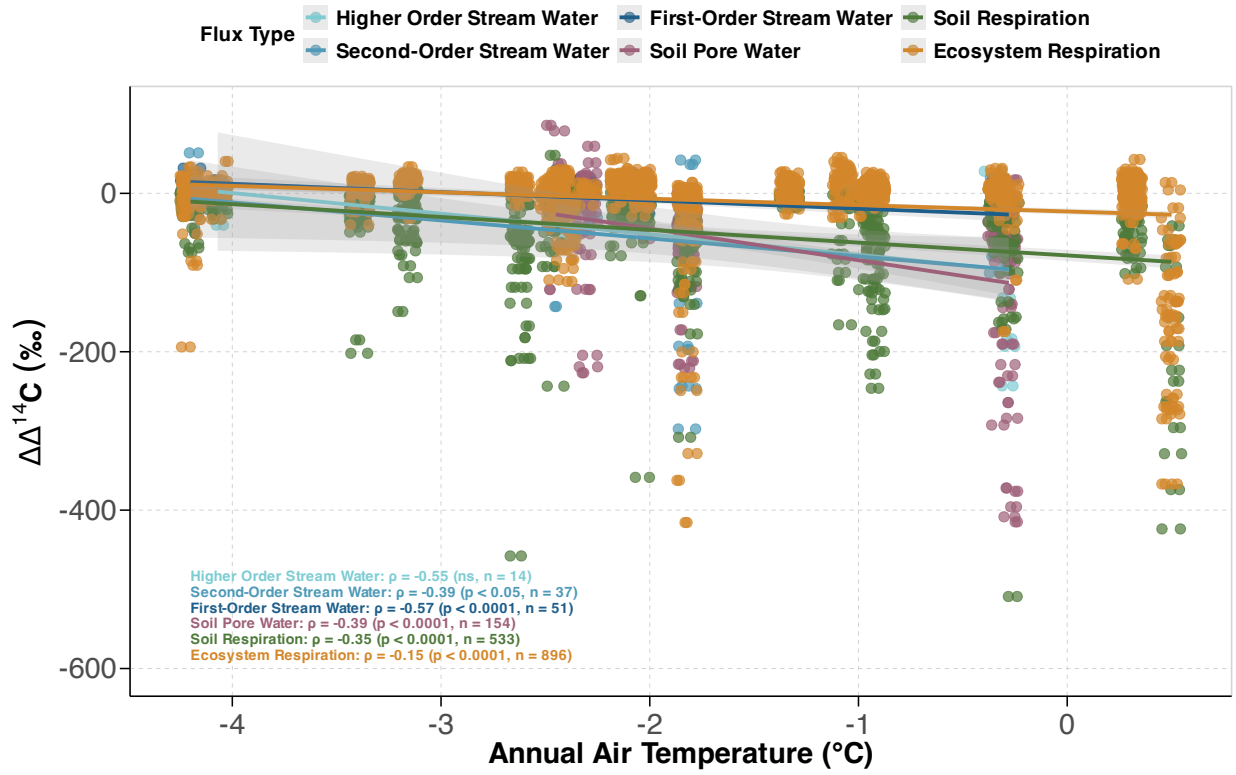
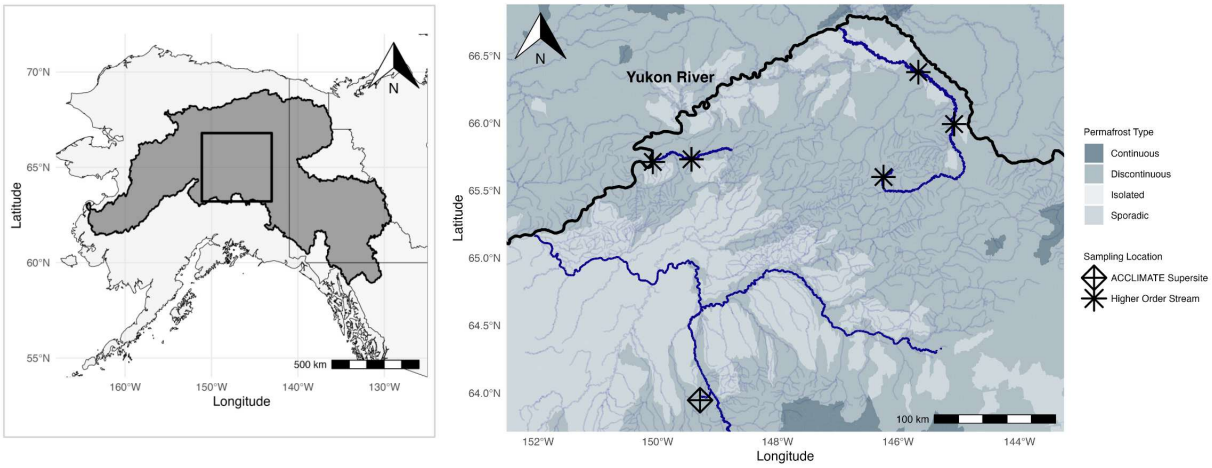


Figure 3: Temperature controls on the radiocarbon age of ecosystem carbon fluxes
Relationships between radiocarbon depletion relative to the atmosphere ($\Delta\Delta^{14}C$) and air temperature across the carbon fluxes. Solid lines indicate linear fits with shaded 95% confidence intervals. Negative relationships between $\Delta\Delta^{14}C$ and temperature indicate enhanced mobilization of older carbon under warmer conditions. $\Delta\Delta^{14}C$ represents the sample $\Delta^{14}C$ deviation from atmospheric radiocarbon in the year of sample collection to allow for the comparison across years.

Materials and Methods

Site Context

Our objective was to quantify patterns of radiocarbon release in both terrestrial and aquatic fluxes across the discontinuous permafrost zone. We compiled high-frequency time series from the long-term permafrost observatory ACCLIMATE and integrated these with multi-decadal records of dissolved organic carbon radiocarbon (^{14}C-DOC) from rivers within the Yukon River watershed. By coupling intensive, site-level observations with regional riverine datasets, we assessed whether temporal trends observed locally were reflected at regional scales. To extend the temporal coverage of the riverine record, we re-sampled previously published sites and updated the ^{14}C-DOC time series through 2024.



The ACCLIMATE observatory is located in the Eight Mile Lake watershed near Healy, Alaska (63°52'59"N, 149°13'32"W), within the discontinuous permafrost zone (50–90% permafrost cover). The tundra catchment drains via water tracks and first-order streams into Panguingue Creek, a second-order stream within the Yukon River basin. Soils comprise an ~35-cm organic horizon overlying cryoturbated mineral glacial deposits, underlain by permafrost that has undergone rapid thaw in recent decades, including a doubling of active layer thickness since 2009 and sustained ground temperatures above 0 °C at 10 cm depth since 2010. The site includes the long-term Gradient monitoring area (established 2003) and the CiPEHR whole-ecosystem warming experiment (established 2008), enabling comparison of natural and experimentally accelerated thaw[47–49].

We incorporated previously published and newly extended radiocarbon datasets from the Birch Creek and Hess Creek watersheds, both major tributaries within the Yukon River basin and located in the discontinuous permafrost zone of interior Alaska. These catchments encompass contrasting geomorphic and permafrost settings, including upland headwaters, ice-rich Yedoma deposits, peat-rich lowlands, and areas of locally continuous permafrost[50]. Stream water samples were collected seasonally (2002-2011) and analyzed

for $\Delta^{14}C$ of bulk DOC using accelerator mass spectrometry. A subset of samples were collected as hydrophobic organic acid (HPOA) isolates rather than bulk DOC. Paired comparison at co-sampled sites (n = 5 pairs) showed no significant difference in $\Delta^{14}C$ between sample types (mean difference = 5.4 ± 12.3‰, paired t-test p = 0.38), with no proportional bias across the measured range (Bland-Altman analysis) and slope estimates differing by less than 0.1‰ yr^{-1} with or without HPOA inclusion. HPOA isolates were therefore treated as equivalent to bulk DOC.

At ACCLIMATE, we quantified radiocarbon signatures of terrestrial carbon exported within respiration fluxes (soil respiration CO_2 and ecosystem respiration CO_2) and aquatically (soil pore water DOC, first-order stream DOC, and second-order stream DOC, Panguingue Creek). At this site, soil pore water (~0.5 m depth) drains via water tracks into headwater streams and subsequently into the second-order stream, Panguingue Creek, providing a hillslope-to-stream continuum. Water samples were collected during the growing season (June-September), excluding snowmelt and large storm events. Soil pore water was sampled from permanent wells (n = 45), purged prior to collection, filtered (0.7 µm GF/F pre-ashed filters), acidified (pH<2), and stored refrigerated or frozen until analysis. In 2023 and 2024, additional samples were obtained using macro-rhizon samplers. Stream sites were sampled episodically (2007-2016) and weekly during selected growing seasons (2017, 2020-2024). Soil respiration $\Delta^{14}CO_2$ (2003-2024) was measured using soil gas wells and passive samplers, and ecosystem respiration $\Delta^{14}CO_2$ was quantified using flow-through chamber methods.

Laboratory Radiocarbon Analyses

Samples collected after 2019 were analyzed at the Arizona Climate and Ecosystems (ACE) Isotope Laboratory (Northern Arizona University) and samples from previous years were analyzed at the UC Irvine W. M. Keck Carbon Cycle Accelerator Mass Spectrometry Laboratory (University of California Irvine).

CO_2 samples were recovered from molecular sieve traps by heating to 625 °C, purified, graphitized, and measured for ^{14}C by accelerator mass spectrometry[51]. Ecosystem respiration samples were additionally analyzed for $\delta^{13}C$ to correct for atmospheric CO_2 intrusion using $^{13}C/^{12}C$ ratios; soil respiration samples did not require this correction[15]. Annual plant material was graphitized and analyzed for ^{14}C using identical procedures to determine the annual, atmospheric radiocarbon signal.

DOC samples collected between 2020 and 2024 were oxidized to CO_2 via wet chemical oxidation and analyzed on a Miniaturized Carbon Dating System (MICADAS) equipped with a carbonate handling system (CHS2) and gas interface system (GIS)[52]. Pre-2020 DOC samples were concentrated by rotary evaporation, combusted at 900 °C in

sealed quartz tubes with CuO and Ag, cryogenically purified, and reduced to graphite by iron reduction prior to ^{14}C measurement[53].

Radiocarbon measurements were calibrated using gas OX-II standards and ^{14}C-dead CO_2 (IonPlus, Switzerland). For each analytical run, four to five OX-II replicates (SD = 6.8‰) and three process blanks (mean radiocarbon age ≈ 38,800 yr) were included. Replicate analyses of an internal DOC reference material were performed on each day of measurement (n = 16 total), yielding a standard deviation of 7.5‰. Analytical uncertainty for $\Delta^{14}C$ measurements was approximately ±8‰.

Statistical Analyses

Temporal trends in $\Delta^{14}C$ were estimated for each carbon flux type using linear regression. For flux types with repeated measures structure, where five or more distinct samples were measured across more than two years on average and fewer than 50% of samples were measured only once or twice (ecosystem respiration and soil respiration), we used linear mixed-effects models (lme) with a random intercept per sample to account for non-independence of repeated observations (lme, nlme package). For flux types that were largely cross-sectional (higher-order stream, second-order stream, first-order stream, and soil pore water DOC), we used ordinary least squares (lm) or generalized least squares (gls) regressions. For all models, we tested whether a variance-exponential error structure (varExp) or an additional AR(1) autocorrelation term (corAR1) improved fit relative to the base model using AIC; the corAR1 structure was retained only if ΔAIC > 5 relative to the varExp model.

To compare flux-specific slopes against the contemporaneous atmospheric decline, we fit a separate atmospheric linear model over the timeseries. A more negative slope compared to the atmosphere would indicate an increase in old C presence. A one-tailed Z-test was then used to evaluate whether each flux slope was significantly more negative than the atmospheric slope:

$$z = \frac{\beta_{1,\text{flux}} - \beta_{1,\text{atm}}}{\sqrt{SE_{\text{flux}}^2 + SE_{\text{atm}}^2}}$$

where SE denotes the standard error of the fitted slope. One-tailed p values were obtained from the standard normal distribution.

To evaluate whether temporal trends differed among flux types, we conducted pairwise two-tailed Z-tests between all flux slope pairs, with p-values adjusted for multiple comparisons using the Benjamini-Hochberg (BH) procedure. Compact letter displays were generated from adjusted p-values to summarize groupings (Table S1; Fig. S1).

To assess the relationship between $\Delta\Delta^{14}C$ (flux $\Delta^{14}C$ minus contemporaneous atmospheric $\Delta^{14}C$) and air temperature, we used Spearman rank correlations. Temperature

was obtained from the ACCLIMATE HOBO weather station (2004 to 2024) and was gap-filled for 2002 to 2003 using a bias-corrected linear model trained on overlapping years with NOAA Alaska Climate Division 3 data. Correlations were evaluated for growing season (May through September), non-growing season (October through April), and annual mean temperature (Fig. S5) using both NOAA Alaska Climate Division 3 data and ACCLIMATE Site data. P-values were adjusted for multiple comparisons across flux type and temperature source combinations using the BH procedure. Annual air temperatures for this region are presented in Figure S6.

We also estimated the proportional contributions of two carbon sources, young carbon (combining surface soils, plant material, and post-1960s bomb carbon) and deep soil carbon (below 45 cm)[54], to the ecosystem carbon fluxes using Bayesian isotope mixing models. For each flux, we modeled the radiocarbon signal as a function of year to quantify temporal trends in source contributions, including process error in all models. Uniform (flat) Dirichlet priors were used for all source proportions, allowing the data to drive posterior estimates without informative prior assumptions about source contributions. Higher order stream DOC was modeled using a two-period factor model comparing the early sampling period (2005-2010) to recent observations (2024), rather than a continuous temporal trend, due to the 13-year gap in sampling. Model outputs in isometric log-ratio space were back-transformed to source proportions and summarized using median values and 95% credible intervals. Convergence was confirmed using the Gelman-Rubin diagnostic ($\hat{R}<1.01$ for all parameters across all models) and visual inspection of traceplots.

Extended Data

Table S1

Dependent Variable	Slope ± SE (‰ yr^{-1})	Z-score	Z-Test p-value	Pairwise Group	Years	n
Higher-Order Stream Δ^{14}C-DOC	-12.2 ± 1.3	-6.3	<0.001 (1.96e-10)	**a**	2002–2024	14
Second-Order Stream Δ^{14}C-DOC	-11.3 ± 2.7	-2.8	<0.01 (2.90e-03)	**ab**	2012–2024	37
First-Order Stream Δ^{14}C-DOC	-5.2 ± 0.5	-2.9	<0.01 (2.16e-03)	**b**	2007–2024	51
Soil Pore Δ^{14}C-DOC	-15.6 ± 2.7	-4.3	<0.001 (8.34e-06)	**a**	2016–2024	159
Soil Respiration $\Delta^{14}CO_2$	-6.6 ± 0.5	-5.3	<0.001 (7.18e-08)	**b**	2004–2024	534
Ecosystem Respiration $\Delta^{14}CO_2$	-6.3 ± 0.2	-11.0	<0.001 (2.01e-28)	**b**	2003–2024	896

Slopes±SE from best-fit linear models (linear regression, GLS, or linear mixed-effects with random intercept per sample, selected by AIC) with Year as a predictor of Δ^{14}C. P-values are from one-tailed Z-tests (α = 0.05) testing the a priori hypothesis that each flux slope was more negative than the contemporaneous atmospheric decline (-3.8±0.1‰ yr^{-1})[55,56], indicating increasing incorporation of old carbon over time, outpacing the incorporation of fossil fuel old carbon causing the atmospheric decline. Pairwise grouping letters are from BH-adjusted two-tailed Z-tests; fluxes sharing a letter are not significantly different from one another.

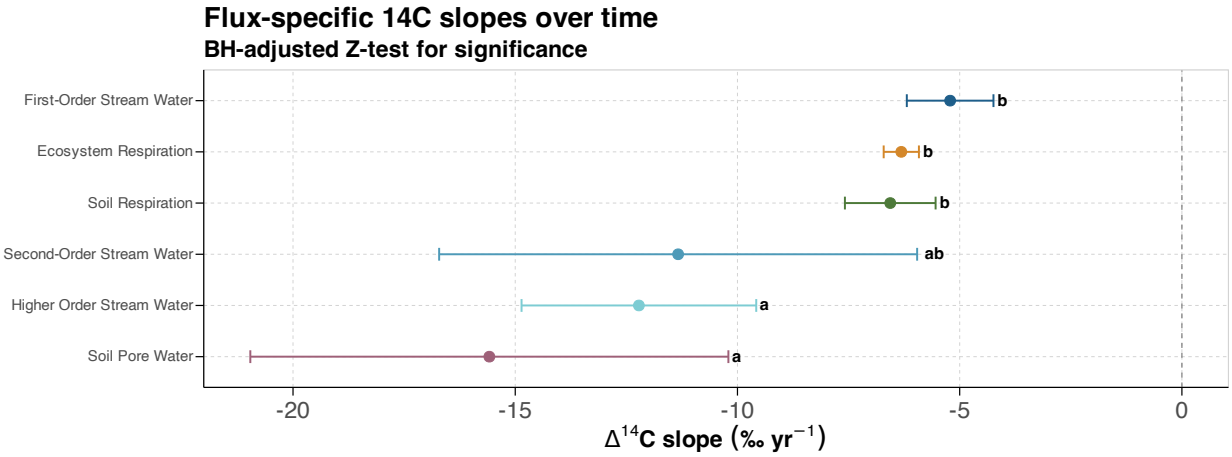


Figure S1. Flux-specific Δ^{14}C slopes over time.
Points represent slope estimates (‰ yr^{-1}) with 95% confidence intervals. Compact letter display indicates results of pairwise two-tailed Z-tests with Benjamini-Hochberg correction; flux types sharing a letter are not significantly different from one another (p > 0.05).

Radiocarbon declined over time across all carbon flux types, but the rate of decline varied (Fig. 1, S1; Table S1). Pairwise comparisons indicated that higher-order stream DOC and

soil pore DOC (group “a”) declined significantly faster than first-order stream DOC, ecosystem respiration, and soil respiration (group “b”). Second-order stream DOC (group “ab”) exhibited an intermediate rate of decline and was not significantly different from either the faster- or slower-declining groups.

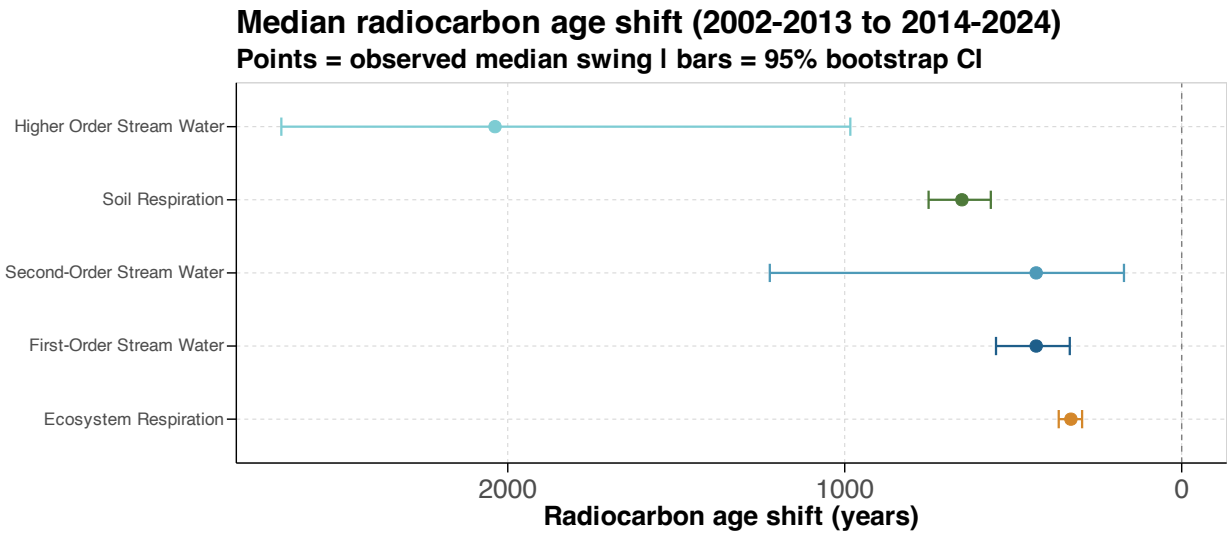
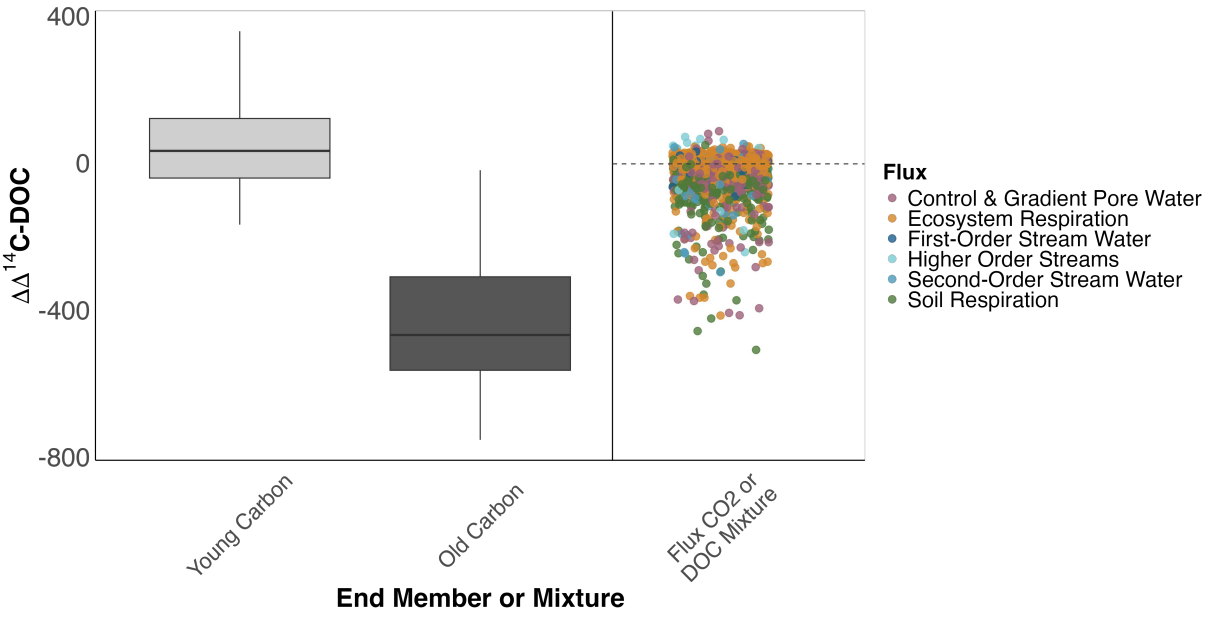


Figure S2. Median radiocarbon age shifts between the first and second halves of the timeseries *Shift in median radiocarbon age between the early (2002–2013) and late (2014-2024) periods for each flux type. Points show the observed difference in median radiocarbon age (years BP); horizontal bars show 95% bootstrap confidence intervals (n = 1,000 iterations). Positive values indicate that carbon exported in the later period was older on average. Soil pore water is excluded due to a lack of observations prior to 2016.*

The observed shift in median radiocarbon age between periods (late - early) was calculated for each flux, and uncertainty was estimated using a nonparametric bootstrap (n = 1,000 iterations) to generate 95% confidence intervals around the median.



412

413 **Figure S3. End member and flux radiocarbon distributions**
414 *The left panel presents young and old carbon end member distributions as boxplots. These end members*
415 *were used in the Bayesian mixing model to estimate the relative contributions of each end member source to*
416 *the radiocarbon signature of the fluxes ($\Delta\Delta^{14}C\text{-}CO_2$ and $\Delta\Delta^{14}C$-DOC, right panel).*

Table S2

Flux	Start Year	End Year	Start Mean Δ14C±SD (‰)	End Mean Δ14C±SD (‰)	End Member	Start Mean ± SD (95% CI) %	End Mean ± SD (95% CI) %	Change (%)
Higher-Order Stream Δ^{14}C-DOC	2002–2011†	2024	-16.0±32.0	-165.2±64.5	**Old Carbon**	**20 ± 8 (6–35)**	**37 ± 14 (8–64)**	**+17**
					Young Carbon	80 ± 8 (65–94)	63 ± 14 (36–92)	-17
Second-Order Stream Δ^{14}C-DOC	2012	2024	-0.1±31.9	-74.9±22.2	**Old Carbon**	**10 ± 16 (0–60)**	**50 ± 24 (10–95)‡**	**+40**
					Young Carbon	90 ± 16 (40–100)	50 ± 24 (5–90)‡	-40
First-Order Stream Δ^{14}C-DOC	2007	2024	7.4±6.9	-25.7±3.2	**Old Carbon**	**13 ± 23 (0–88)**	**48 ± 33 (2–100)‡**	**+35**
					Young Carbon	87 ± 23 (12–100)	52 ± 33 (0–98)‡	-35
Soil Pore Δ^{14}C-DOC	2016	2024	-44.6±58.9	-148.1±138.3	**Old Carbon**	**6 ± 4 (1–15)**	**56 ± 10 (35–77)**	**+50**
					Young Carbon	94 ± 4 (85–99)	44 ± 10 (23–65)	-50
Ecosystem Respiration $\Delta^{14}CO_2$	2003	2024	11.9±20.3	-34.1±54.8	**Old Carbon**	**2 ± 1 (1–4)**	**62 ± 10 (42–81)**	**+60**
					Young Carbon	98 ± 1 (96–99)	38 ± 10 (19–58)	-60
Soil Respiration $\Delta^{14}CO_2$	2004	2024	-67.7±71.9	-107.4±106.3	**Old Carbon**	**5 ± 2 (3–9)**	**80 ± 8 (61–92)**	**+74**
					Young Carbon	95 ± 2 (91–97)	20 ± 8 (8–39)	-74

Modeled contributions of Old Carbon and Young Carbon to each flux at the start and end of the study period, with net change. Observed $\Delta^{14}C$ values (mean±sd) shown for the start and end periods to contextualize model results. Model mean and 95% credible intervals expressed as percent contribution.

† Higher Order Streams: two-period factor model comparing Early (2005-2011) vs. Recent (2024) periods due to 13-year sampling gap; temporal trend not fitted. ‡ Wide credible intervals reflect genuine high variance in stream water $\Delta^{14}C$ (sd > 80‰).

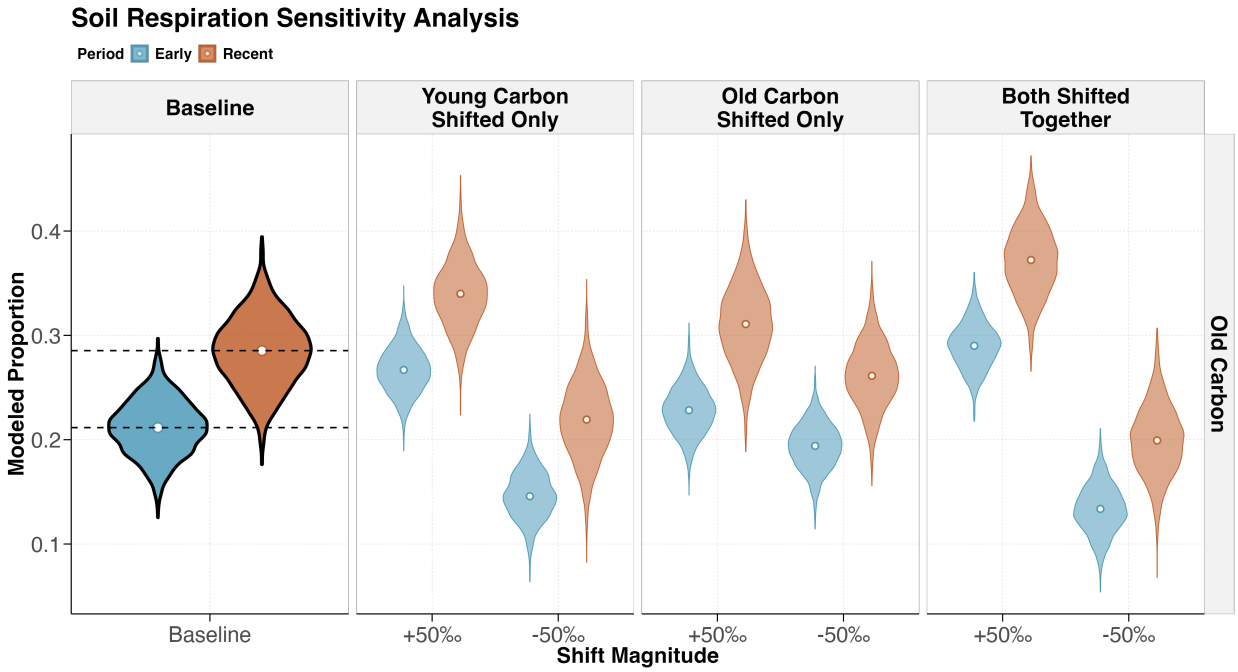


Figure S4. Sensitivity of modeled old carbon proportions in soil respiration to end-member isotopic uncertainty.
Violin plots show posterior distributions of old carbon contributions to soil respiration for early (blue; 2002-2004) and recent (orange; 2022-2024) periods across seven scenarios in which young carbon, old carbon, or both end-members were shifted by ±50‰. Points indicate posterior means. The recent period consistently shows higher old carbon proportions than the early period across all scenarios, demonstrating robustness to end-member uncertainty.

To evaluate how uncertainty in radiocarbon ($\Delta^{14}C$) end-member values affects modeled source proportions, we conducted a sensitivity analysis using MixSIAR by systematically perturbing the isotopic values of the two-source end-members: young carbon and old carbon. We applied shifts of ±50‰ to each end-member independently and in combination, yielding seven scenarios: a baseline (no shift), young carbon shifted alone (+50‰, -50‰), old carbon shifted alone (+50‰, -50‰), and both end-members shifted simultaneously in the same direction (+50‰, -50‰). Each scenario was run as a two-source Bayesian mixing model in MixSIAR, with a fixed categorical factor distinguishing the early period (first three years: 2002–2004) from the recent period (last three years: 2022–2024) of the timeseries, to detect if the shifts observed across the timeseries were detectable. Posterior distributions of source proportions were approximated from the mean and 95% credible intervals of each model output assuming a Gaussian distribution (n = 3,000 draws per scenario), and results were visualized as violin plots comparing early and recent periods across all perturbation scenarios.

Across all seven perturbation scenarios, the modeled proportion of old carbon in soil respiration was consistently higher in the recent period than in the early period, regardless of the direction or magnitude of end-member shifts applied, indicating that the observed increase in old carbon contribution to soil respiration over the timeseries is robust to uncertainty in end-member isotopic values. The separation between early and recent posterior distributions was maintained across all scenarios, supporting the conclusion that the shift toward greater old carbon proportions reflects a real biogeochemical signal rather than an artifact of end-member parameterization.

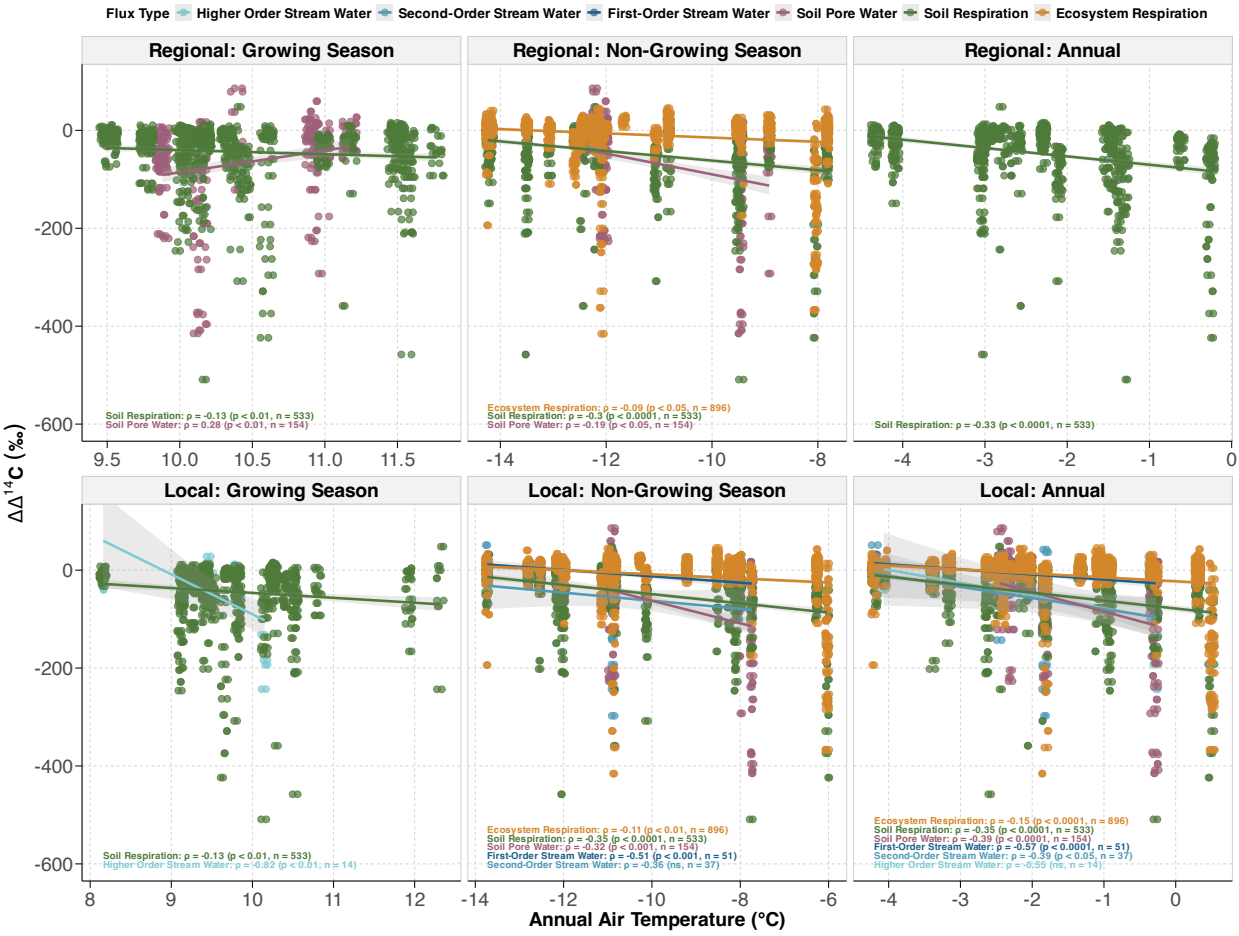


Figure S5: Temperature controls on the radiocarbon age of ecosystem carbon fluxes
Relationships between radiocarbon depletion relative to the atmosphere ($\Delta\Delta^{14}C$) and air temperature for carbon fluxes showing statistically significant correlations (Spearman's ρ, BH-adjusted p<0.05, n ≥ 5). Panels show regional (NOAA Alaska Division 3) and local (Healy station, gap-filled for 2002–2003 using bias-corrected regional data) temperature across growing season (May-September), non-growing season (October–April), and annual means. Lines indicate linear fits with shaded 95% confidence intervals. Negative relationships between $\Delta\Delta^{14}C$ and temperature indicate enhanced mobilization of older carbon under warmer conditions. Only flux x temperature combinations meeting the minimum sample threshold are shown.

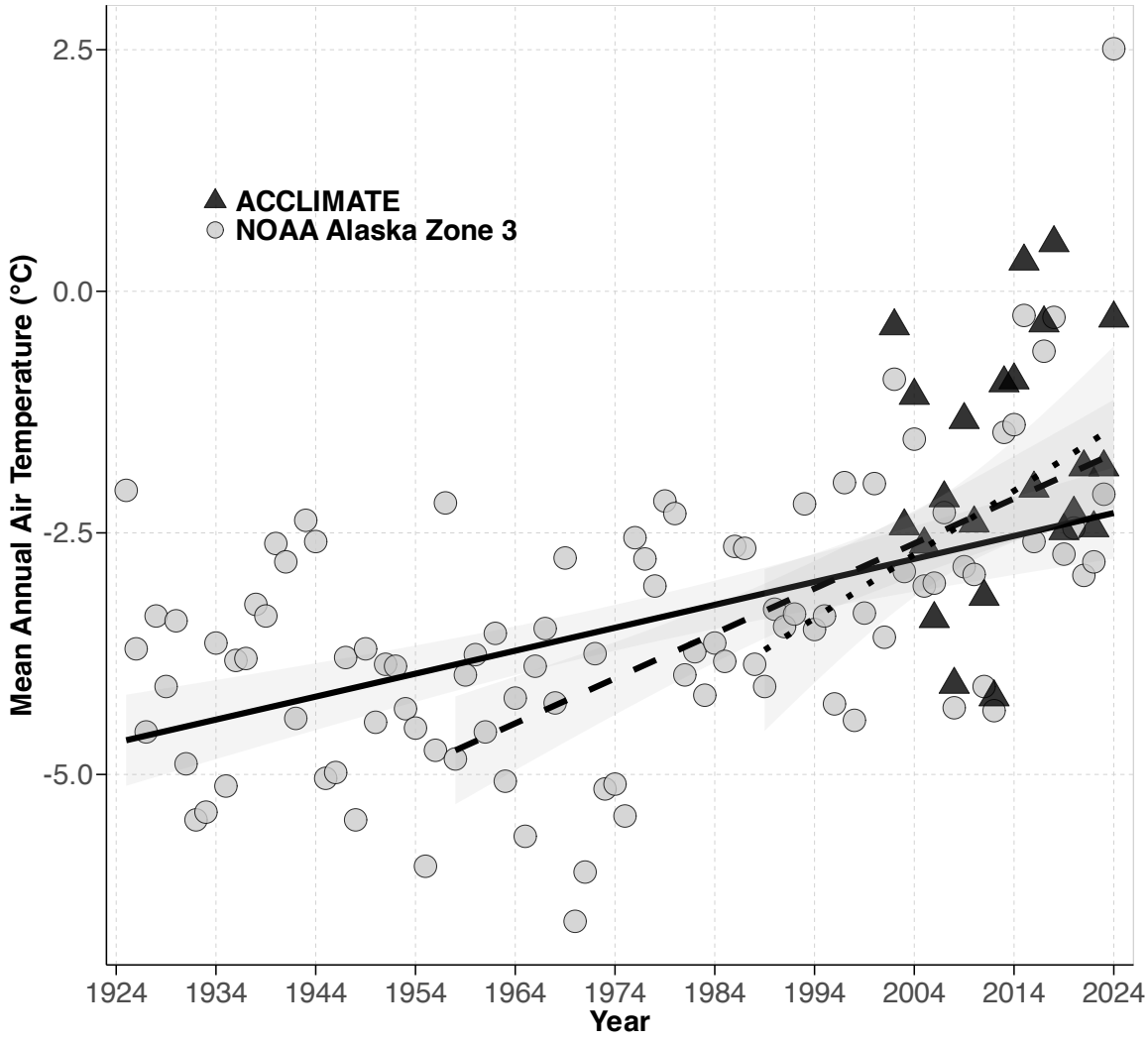


Figure S6: Mean annual air temperature for the NOAA AKCD3 Region from 1925-2024 and for the ACCLIMATE study site from 2004-2024.
The solid line represents the average increase in temperature since 1925; dashed line since 1958; dotted line since 1989. All line fits are statistically significant based on the AKCD3 data set, NOAA, National Oceanic and Atmospheric Administration.

Mean annual air temperature in Interior Alaska increased at a rate of 0.24°C decade^{-1} since 1925, accelerating to 0.47 °C decade^{-1} since 1958, and to 0.66 °C decade^{-1} since 1989 (all $p<0.01$), consistent with amplified Arctic warming in recent decades.

References

1. Schuur, E. A. G. *et al.* Climate change and the permafrost carbon feedback. *Nature* **520**, 171–179 (2015).
2. Schuur, E. A. G. & Mack, M. C. Ecological Response to Permafrost Thaw and Consequences for Local and Global Ecosystem Services. *Annual Review of Ecology and Systematics* **49**, 279–301 (2018).
3. Schuur, E. A. G. *et al.* Permafrost and Climate Change: Carbon Cycle Feedbacks From the Warming Arctic. *Annu. Rev. Environ. Resour.* **47**, 343–371 (2022).
4. Rantanen, M. *et al.* The Arctic has warmed nearly four times faster than the globe since 1979. *Commun Earth Environ* **3**, 1–10 (2022).
5. Miner, K. R. *et al.* Permafrost carbon emissions in a changing Arctic. *Nat Rev Earth Environ* **3**, 55–67 (2022).
6. Natali, S. M. *et al.* Permafrost carbon feedbacks threaten global climate goals. *PNAS* **118**, (2021).
7. Koven, C. *et al.* Permafrost carbon-climate feedbacks accelerate global warming. *Proceedings of the National Academy of Sciences USA* **108**, 14769–14774 (2011).
8. Ciais, P. *et al.* Carbon and Other Biogeochemical Cycles. in *Climate Change 2013: The Physical Science Basis. Contribution of Working Group I to the Fifth Assessment Report of the Intergovernmental Panel on Climate Change* (eds Stocker, T. F. et al.) (Cambridge University Press, Cambridge, United Kingdom and New York, NY, USA, 2013).

9. Lawrence, D. M., Koven, C. D., Swenson, S. C., Riley, W. J. & Slater, A. G. Permafrost thaw and resulting soil moisture changes regulate projected high-latitude CO_2 and CH_4 emissions. *Environ. Res. Lett.* **10**, 094011 (2015).
10. Schaefer, K., Lantuit, H., Romanovsky, V. E., Schuur, E. A. G. & Witt, R. The impact of the permafrost carbon feedback on global climate. *Environmental Research Letters* **9**, 085003 (2014).
11. Kelley, A. K. *et al.* Lateral Dissolved Organic Carbon Losses Represent ~10% of Upland Tundra Carbon Losses and Include Seasonal Permafrost Contributions. *Journal of Geophysical Research: Biogeosciences* **130**, e2025JG009067 (2025).
12. Czimczik, C. I. & Welker, J. M. Radiocarbon content of CO2 respired from high Arctic tundra in northwest Greenland. *Arctic Antarctic and Alpine Research* **42**, 342–350 (2010).
13. Schuur, E. A. G. & Trumbore, S. E. Partitioning sources of soil respiration in boreal black spruce forest using radiocarbon. *Global Change Biology* **12**, 165–176 (2006).
14. Estop-Aragonés, C. *et al.* Assessing the Potential for Mobilization of Old Soil Carbon After Permafrost Thaw: A Synthesis of 14C Measurements From the Northern Permafrost Region. *Global Biogeochemical Cycles* **34**, e2020GB006672 (2020).
15. Schuur, E. A. G. *et al.* Ecosystem and soil respiration radiocarbon detects old carbon release as a fingerprint of warming and permafrost destabilization with climate change. *Philosophical Transactions of the Royal Society A: Mathematical, Physical and Engineering Sciences* **381**, 20220201 (2023).

16. Trumbore, S. Carbon respired by terrestrial ecosystems - recent progress and challenges. *Global Change Biology* **12**, 141–153 (2006).
17. Dean, J. F. *et al.* Old carbon routed from land to the atmosphere by global river systems. *Nature* **642**, 105–111 (2025).
18. Sierra, C. A., Müller, M., Metzler, H., Manzoni, S. & Trumbore, S. E. The muddle of ages, turnover, transit, and residence times in the carbon cycle. *Global Change Biology* **23**, 1763–1773 (2017).
19. Dean, J. F., Garnett, M. H., Spyrakos, E. & Billett, M. F. The Potential Hidden Age of Dissolved Organic Carbon Exported by Peatland Streams. *Journal of Geophysical Research: Biogeosciences* **124**, 328–341 (2019).
20. Hicks Pries, C. E., Schuur, E. A. G., Natali, S. M. & Crummer, K. G. Old soil carbon losses increase with ecosystem respiration in experimentally thawed tundra. *Nature Clim Change* **6**, 214–218 (2016).
21. Libby, W. F., Anderson, E. C. & Arnold, J. R. Age Determination by Radiocarbon Content - Worldwide Assay of Natural Radiocarbon. *Science* **109**, 227–228 (1949).
22. *Radiocarbon and Climate Change: Mechanisms, Applications and Laboratory Techniques*. (Springer, 2016).
23. Trumbore, S. Age of Soil Organic Matter and Soil Respiration: Radiocarbon Constraints on Belowground C Dynamics. *Ecol Appl* **10**, 399–411 (2000).
24. Marshall, L. P., Kaufman, D. S., Anderson, R. S., McKay, N. P. & Schuur, E. A. G. Organic-Matter Accumulation and Degradation in Holocene Permafrost Deposits Along a

Central Alaska Hillslope. *Journal of Geophysical Research: Biogeosciences* **128**, e2022JG007290 (2023).

25. Mauritz, M., Pegoraro, E., Ogle, K., Ebert, C. & Schuur, E. A. G. Investigating Thaw and Plant Productivity Constraints on Old Soil Carbon Respiration From Permafrost. *Journal of Geophysical Research: Biogeosciences* **126**, e2020JG006000 (2021).
26. O'Donnell, J. A. *et al.* Permafrost Hydrology Drives the Assimilation of Old Carbon by Stream Food Webs in the Arctic. *Ecosystems* **23**, 435–453 (2020).
27. Aiken, G. R., Spencer, R. G. M., Striegl, R. G., Schuster, P. F. & Raymond, P. A. Influences of glacier melt and permafrost thaw on the age of dissolved organic carbon in the Yukon River basin. *Global Biogeochemical Cycles* **28**, 525–537 (2014).
28. Pedron, S. A. *et al.* Closing the Winter Gap—Year-Round Measurements of Soil CO2 Emission Sources in Arctic Tundra. *Geophysical Research Letters* **49**, e2021GL097347 (2022).
29. Graven, H. D. Impact of fossil fuel emissions on atmospheric radiocarbon and various applications of radiocarbon over this century. *Proceedings of the National Academy of Sciences* **112**, 9542–9545 (2015).
30. Xu, X. Atmospheric 14CO2 time series from Point Barrow, Alaska: ending of the 'Bomb Radiocarbon Period' in the Northern Hemisphere. (2022).
31. Kelley, A. K. *et al.* Eight Mile Lake Research Watershed, Carbon in Permafrost Experimental Heating Research (CiPEHR): Weekly thaw depth data, 2009-2023. Environmental Data Initiative https://doi.org/10.6073/PASTA/C0007764015FAC9AFB4EB4ABCC9D9E4D (2024).

32. Pegoraro, E. F., Mauritz, M. E., Ogle, K., Ebert, C. H. & Schuur, E. A. G. Lower soil moisture and deep soil temperatures in thermokarst features increase old soil carbon loss after 10 years of experimental permafrost warming. *Glob. Change Biol.* **27**, 1293–1308 (2021).
33. Vonk, J. E. *et al.* Biodegradability of dissolved organic carbon in permafrost soils and aquatic systems: a meta-analysis. *Biogeosciences* **12**, 6915–6930 (2015).
34. Kelley, A. K. *et al.* Permafrost thaw exposes old dissolved organic carbon to photo- and biodegradation. *Environ. Res.: Ecology* **5**, 015003 (2026).
35. Kelley, A. K. *et al.* Permafrost thaw exposes old dissolved organic carbon to photo- and biodegradation. *Environ. Res.: Ecology* **5**, 015003 (2026).
36. Spencer, R. G. M. *et al.* Detecting the signature of permafrost thaw in Arctic rivers. *Geophysical Research Letters* **42**, 2830–2835 (2015).
37. Neff, J. C. *et al.* Seasonal changes in the age and structure of dissolved organic carbon in Siberian rivers and streams. *Geophysical Research Letters* **33**, (2006).
38. Raymond, P. A. *et al.* Flux and age of dissolved organic carbon exported to the Arctic Ocean: A carbon isotopic study of the five largest arctic rivers. *Global Biogeochemical Cycles* **21**, (2007).
39. Biskaborn, B. K. *et al.* Permafrost is warming at a global scale. *Nat Commun* **10**, 264 (2019).
40. Pedron, S. A. *et al.* More Snow Accelerates Legacy Carbon Emissions From Arctic Permafrost. *AGU Advances* **4**, e2023AV000942 (2023).

41. Hicks Pries, C. E., Schuur, E. A. G. & Crummer, K. G. Thawing permafrost increases old soil and autotrophic respiration in tundra: Partitioning ecosystem respiration using δ13C and Δ14C. *Global Change Biology* **19**, 649–661 (2013).
42. Chen, Y. *et al.* Large-scale evidence for microbial response and associated carbon release after permafrost thaw. *Global Change Biology* **27**, 3218–3229 (2021).
43. Feng, J. *et al.* Warming-induced permafrost thaw exacerbates tundra soil carbon decomposition mediated by microbial community. *Microbiome* **8**, 3 (2020).
44. Walvoord, M. & Kurylyk, B. Hydrologic Impacts of Thawing Permafrost-A Review. *Vadose Zone Journal* **15**, (2016).
45. Sjöberg, Y. *et al.* Permafrost Promotes Shallow Groundwater Flow and Warmer Headwater Streams. *Water Resources Research* **57**, e2020WR027463 (2021).
46. Welch, A. C. *et al.* Eight Mile Lake Research Watershed, Carbon in Permafrost Experimental Heating Research (CiPEHR): Weekly thaw depth data, 2009-2025. Environmental Data Initiative https://doi.org/10.6073/PASTA/B802CEF9820B9D929E93D382419561E3 (2026).
47. Schuur, E. A. G. *et al.* Tundra Underlain By Thawing Permafrost Persistently Emits Carbon to the Atmosphere Over 15 Years of Measurements. *J Geophys Res Biogeosci* **126**, (2021).
48. Plaza, C. *et al.* Direct observation of permafrost degradation and rapid soil carbon loss in tundra. *Nature Geoscience* **12**, 627–631 (2019).
49. Schuur, E. A. G. *et al.* The effect of permafrost thaw on old carbon release and net carbon exchange from tundra. *Nature* **459**, 556–559 (2009).

50. O'Donnell, J. A. *et al.* Using dissolved organic matter age and composition to detect permafrost thaw in boreal watersheds of interior Alaska. *Journal of Geophysical Research: Biogeosciences* **119**, 2155–2170 (2014).
51. Bauer, J. E., Williams, P. M. & Druffel, E. R. M. Recovery of Submilligram Quantities of Carbon-Dioxide from Gas Streams by Molecular-Sieve for Subsequent Determination of Isotopic (C-13 and C-14) Natural Abundances. *Anal Chem Anal Chem* **64**, 824–827 (1992).
52. Lang, S. Q. *et al.* Rapid 14C Analysis of Dissolved Organic Carbon in Non-Saline Waters. *Radiocarbon* **58**, 505–515 (2016).
53. Vogel, J. S., Southon, J. R., Nelson, D. E. & Brown, T. A. Performance of catalytically condensed carbon for use in Accelerator Mass-Spectrometry. *Nuclear Instruments & Methods in Physics Research Section B-Beam Interactions with Materials and Atoms* **5**, 289–293 (1984).
54. Lathrop, E. R. *et al.* Eight Mile Lake Research Watershed, Carbon in Permafrost Experimental Heating Research (CiPEHR): soil organic carbon stocks and radiocarbon measurements, 2009 & 2022. Environmental Data Initiative https://doi.org/10.6073/PASTA/27DBA2482BF59890E4397FF6F4352A25 (2025).
55. Hua, Q. *et al.* ATMOSPHERIC RADIOCARBON FOR THE PERIOD 1950–2019. *Radiocarbon* **64**, 723–745 (2022).
56. Ebert, C. H., Schuur, E. A. G., Hicks-Pries, C. E., & Bonanza Creek LTER. Eight Mile Lake Research Watershed, Thaw Gradient, The radiocarbon value of ecosystem respiration,

2004-2016 III: Atm. Environmental Data Initiative

https://doi.org/10.6073/PASTA/A87433EF48A42293E34A9B11964DDEF3 (2017).